Soft Matter

Cite this: *Soft Matter*, 2011, **7**, 9737

www.rsc.org/softmatter

PAPER

Mechanical and thermal stabilities of peptide amphiphile fibres

Maaike van den Heuvel,[a] H. Baptist,[b] P. Venema,[b] E. van der Linden,[b] Dennis W. P. M. Löwik*[a] and Jan C. M. van Hest[a]

Received 11th April 2011, Accepted 31st May 2011
DOI: 10.1039/c1sm05642e

In this study the thermal and mechanical stabilities of self-assembled fibres of palmitoyl functionalized GANPNAAG have been examined. The thermal stability was investigated with circular dichroism, dynamic light scattering and fluorescence measurements monitoring the disassembly upon heating and reassembly upon cooling. The determination of the temperature dependence of the critical aggregation concentration allowed us to estimate the thermodynamic parameters involved in the fibre formation process. The mechanical stability of the fibres was studied using flow-induced birefringence. The peptide based self-assembled structures were found to be thermally stable up to 70 °C, while being fractured by moderate shear flow.

Introduction

In nature many materials are constructed *via* a hierarchical self-assembly process from building blocks kept together by non-covalent interactions. One of the important architectures natural building blocks assemble into are fibres.[1] These superstructures have a great variety of functions in nature; collagen *e.g.* is the main constituent of the extracellular matrix, keeping cells together, whereas actin filaments are responsible for guiding cellular movement. On the other hand, amyloid fibrils are associated with diseases like Alzheimer's and diabetes II. In order to study and to better understand formation and function of protein fibres model systems have been developed based on low molecular weight mimics.

In this respect peptide amphiphiles (PAs) which self-assemble into fibres have gained increasing interest over the years. A lot of research has been performed on the assembly of PAs, on their superstructure, function and response to stimuli such as heat, pH or salt.[2–9] With their relative ease of synthesis, they provide the possibility of mimicking structure and function of proteins without the challenging production that traditionally accompanies these large biomolecules. Furthermore, PA design can conveniently be varied in order to effectively explore the structure–function relationship. The peptide moiety in a PA may be the functional part of a protein, or a motif which guides the assembly into complex superstructures. Generally, these small peptide motifs are soluble, and an additional stabilisation is needed, either to guide the peptides into their active conformation or as a driving force for assembly. Often hydrophobicity is used for this purpose.

One strategy to convey hydrophobicity to a peptide is to attach one or more alkyl chains. One of the first examples of this strategy involved the coupling of two hydrophobic tails on one side and a quaternary ammonium ion on the other side of a single amino acid.[10] These amphiphilic structures assembled into ribbons which folded into helices and tubules. Similar structures with three amino acids instead of just one gave fibres as well,[11] in both water and organic solvents. Although a few studies were performed in organic solvents[12] most of the studies on peptide amphiphiles have been performed in water. For example, the group of Stupp developed a peptide amphiphile which assembles into fibres upon acidification.[13] The assembly was driven by an alkyl tail coupled to four cysteines which enable crosslinking of the structure after assembly.[14] A flexible linker connects this part to a solvent-exposed biofunctional section, which could easily be varied. Hydrogen bonds within the peptide head group have been shown to play an essential role in the assembly of PAs[15] and are in subtle interplay with hydrophobic interactions that allow to tune peptide assembly by *e.g.* increasing stabilization by extending the alkyl chain length.[16–19]

Peptide amphiphile fibres can be applied *in vivo* because of their excellent biocompatibility. Many reported applications of PAs are in the biomedical area,[3] such as their use as MRI contrasting agents,[20,21] for the direction of neurite growth,[22] as hydrogels for tissue engineering[23–25] and cosmetics.[26] To determine the possible scope of applications in which these architectures can be applied, not only structure but also dynamic behaviour is of importance. Thermal stability is an important factor for self-assembled systems. Dynamic architectures may change morphology or disassemble upon heating.[5] Such structural changes could be exploited but could also hamper possible applications. In either case, the thermal behaviour of the

[a]*Radboud University Nijmegen, Institute for Molecules and Materials, Heyendaalseweg 135, 6525 AJ Nijmegen, The Netherlands. E-mail: D.Lowik@science.ru.nl; Fax: +31 24 3653393; Tel: +31 24 3652382*
[b]*Department of Agrotechnology & Food Sciences, Wageningen University, Bomenweg 2, 6703 HD Wageningen, The Netherlands*

self-assembled system should be well known to establish their scope of possible applications. Besides thermal stability also mechanical stability is certainly an—often underestimated—issue. For example, in blood vessels and the extracellular matrix shear rates of 100 s^{-1} to 8000 s^{-1} are present.[27] An effective drug delivery cargo has to withstand these forces without breaking. Moreover, in natural systems such as amyloid fibres and actin filaments, shear force has a large influence on fibre growth and fracture.[27,28] Breakage of amyloid fibres is thought to play a significant role in the growth mechanism of these disease-associated fibrils.[29] The component in the shear force that causes the breakage of the fibres is elongational flow. This force stretches a macromolecule with a parabolic force profile in which the largest force is present in the middle of the fibre.[30,31] These elongational forces can even be large enough to break (covalently bound) polymers such as polystyrene[30] and poly(ethylene glycol).[31] Amyloid fibres[27] and fibres from whey protein isolate[32] are also known to fracture under large enough elongational forces. In contradistinction, a small mechanical disturbance is also known to accelerate fibre growth.[29,33]

In this study the thermal and mechanical stabilities of assemblies of PA **1** are described. This eight amino acid peptide GANPNAAG, coupled to palmitic acid (PA **1**, Fig. 1), assembles into fibres in an aqueous environment and has been studied extensively by our group.[17] The peptide is derived from the CS protein of the malaria parasite *Plasmodium falciparum*.[34] The morphology of the fibrous architectures was studied with transmission electron microscopy (TEM, Fig. 2) and CD spectroscopy.[17] Typically, the peptide amphiphiles pack in a stretched β-sheet structure with intercalating tails.[35] The fibres have been shown to align in a strong magnetic field[36] and to polymerize once diacetylene functionality is introduced in the hydrophobic alkyl chains.[37–39] To investigate the thermal stability we studied the effect of temperature on disassembly and reassembly of the fibres. The corresponding thermodynamic parameters for the assembly process were determined by measuring the critical aggregation concentration as a function of temperature. Next the mechanical stability at room temperature was examined by looking at the effects of shear and elongational flow.

A key characterization technique employed in this study regarding mechanical stability is flow-induced birefringence.[40] This technique is based on the birefringence of optical anisotropic fibres that are aligned by shear flow. In Fig. 3 the set-up of a flow-birefringence experiment is shown. A fibre containing solution is placed in a Couette cell and a laser beam is guided through from top to bottom. Upon rotation of the cell (Fig. 3B), the fibres align in the direction of the shear flow, which results in an increase in birefringence signal, *i.e.* if the fibres are optically anisotropic.[27,41,42] Once the shear flow (rotation) is stopped (D) the fibres relax back to a random orientation. From the decay curve (between D and E) a length distribution of the fibre sample can be determined, as it has been described by Rogers *et al.*[42] In a dynamic system broken fibres can also reassemble to their original length in the absence of flow (between D and F).

The critical aggregation concentration (CAC)

Like all self-assembling molecules, PA **1** is molecularly dissolved up to a concentration called the critical aggregation concentration (CAC). Above this concentration, the additional amphiphiles assemble, leaving the concentration of molecularly dissolved amphiphiles constant. We have attempted to determine the CAC using a number of techniques. First, we turned to fluorescence measurements with DPH (1,6-diphenyl-1,3,5-hexatriene) as a probe. This compound is only fluorescent in a hydrophobic environment and is therefore often employed to determine the CAC of aggregates with a hydrophobic core.[43] A stock solution of DPH in THF was added to each of the samples of a dilution series of the amphiphile. In deviation of the usual protocol, the solution was subsequently heated in order to disassemble the aggregates. This allows, during the following cooling step, the fibres to reform and DPH to insert into the hydrophobic interior during the assembly process. This insertion process was observed to be more efficient than when DPH was added to a solution with preformed fibres, which could be concluded from the much higher final fluorescence intensity. The low insertion efficiency in the absence of a heating step is most likely caused by the screening of the hydrophobic interior from insertion by the densely packed peptide amphiphiles. From the fluorescence measurements on a series of concentrations, a CAC of 44 μg mL^{-1} (48 μM) was derived (Fig. 4).

Because of the structural change in the peptide part of the fibres during assembly and disassembly,[17] also CD measurements could be used as a means to determine the CAC. A concentration range of the amphiphile in Milli-Q water was measured, and the transition from a random coil to a β-sheet was found between 65 and 90 μM. The CD measurements gave the same results in the presence of the fluorescent probe DPH, validating the use of this probe in the fluorescence measurements.

Thermal stability

As has been demonstrated before by us, the fibres disassemble upon heating.[17] This again can be shown with CD spectroscopy monitoring the structural transition of the peptide part of the fibres. The disassembly temperature was derived by measuring the intensity of the 196 nm peak during the heating process, and was found to be about 70 °C.[17] Cooling revealed two transitions of the ellipticity signal—one around 60 °C and one around 30 °C (Fig. 5). The first transition (60 °C) depicts the reformation of the fibrous assemblies. The hysteresis between heating and cooling is most likely an undercooling effect, common in

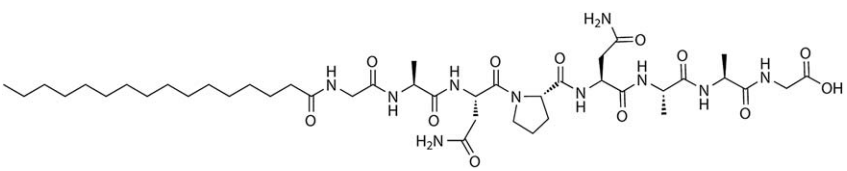

Fig. 1 The structure of the peptide amphiphile in this study, PA **1**.

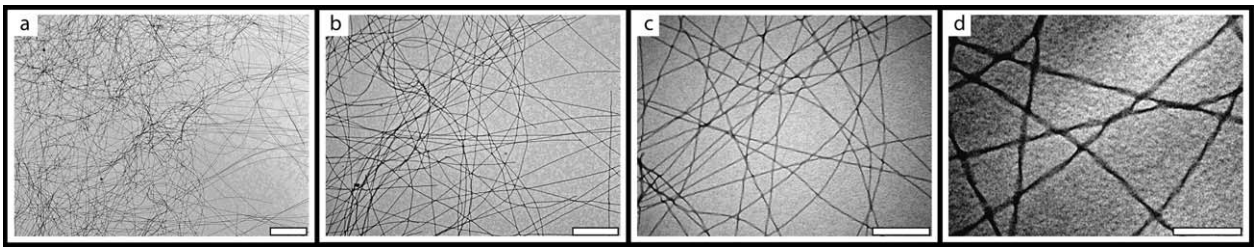

Fig. 2 TEM graphs of PA **1** at different magnifications. The white bars represent (a) 2 μm, (b) 1 μm, (c) 500 nm, and (d) 200 nm.

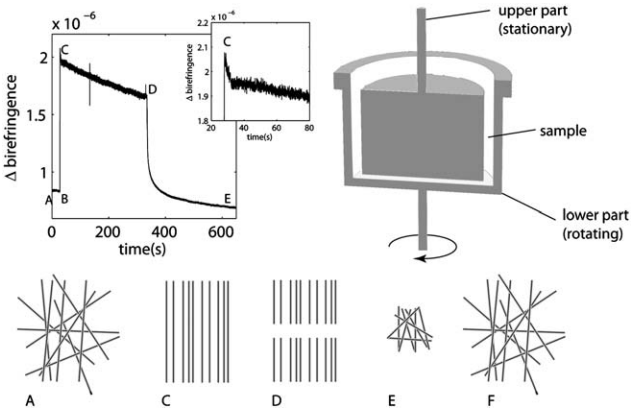

Fig. 3 A typical flow-birefringence experiment. Randomly oriented fibres (A) become aligned (C) caused by shear flow of the Couette cell (upper right corner) that starts to rotate (B), which results in a birefringence signal. Between C and D the Couette cell rotates and the fibres may fracture due to tensile forces as induced by the elongational component of the shear flow. When the shear flow is stopped (D) the fibres relax back to a random orientation (E). The fibres regrow after damage (F), yielding the starting situation (A).

nucleation-induced processes. The second transition temperature (30 °C) is possibly associated with a molecular rearrangement of either alkyl tails or peptides.

The thermal (dis)assembly process was corroborated by DLS measurements determining the total scattering intensity of a fibre sample at different temperatures. The temperature at which the fibres reassembled upon cooling was determined to be 50 °C, *i.e.* the transition point from no assembly to assembly which led to a deviation of the DLS scattering intensity from zero. Upon heating the fibres were found to be completely disassembled at 75 °C (Fig. 6).

Finally, DPH was employed as a fluorescent probe which only fluoresces if fibres are present.[43] The fluorescence intensity of DPH added to the preformed fibres was found to increase abruptly close to 50 °C upon heating (Fig. 7), indicating a larger amount of DPH in a hydrophobic environment. This is most likely caused by a higher conformational freedom of the amphiphiles in the fibres or by a small change in the mobility of the alkyl tails accommodating uptake of DPH in the fibres. After this sudden increase the fluorescence intensity remained constant up to 70 °C after which it decreased drastically, indicating disassembly of the fibres. Upon cooling, the increase in

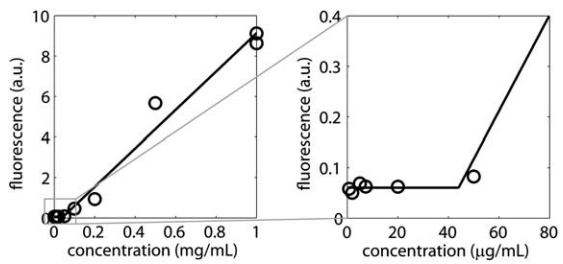

Fig. 4 Determination of the CAC using DPH as a fluorescent probe. The right graph is a magnification of the one on the left for the low concentrations.

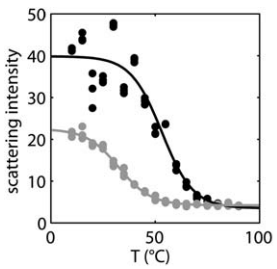

	heating	cooling
inflection point	53 °C	32 °C
assembly onset	~ 75 °C	~ 50 °C

Fig. 6 DLS measurements of PA **1** upon heating (black) and cooling (grey) between 20 and 100 °C. The circles are data points, the lines are fitted sigmoidal curves.

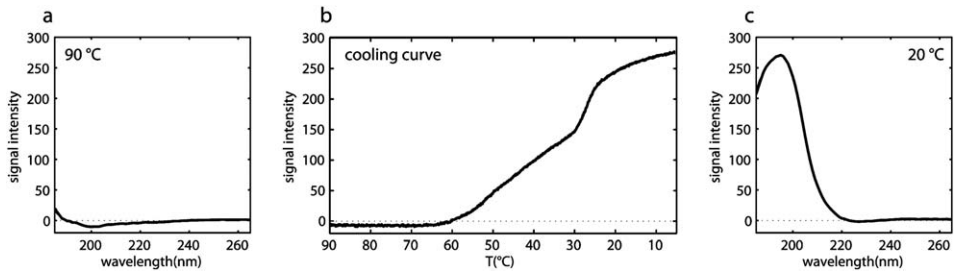

Fig. 5 CD spectra of PA **1** at 90 °C (left) and at 20 °C (right) and the signal intensity at 196 nm upon cooling (middle).

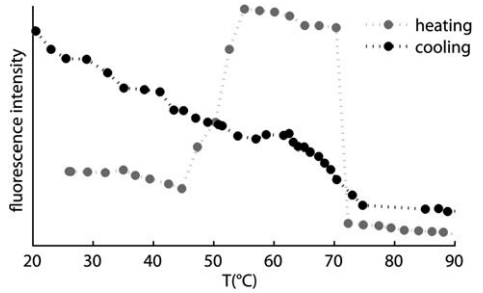

Fig. 7 Fluorescence signal of DPH upon heating and cooling a fibre solution.

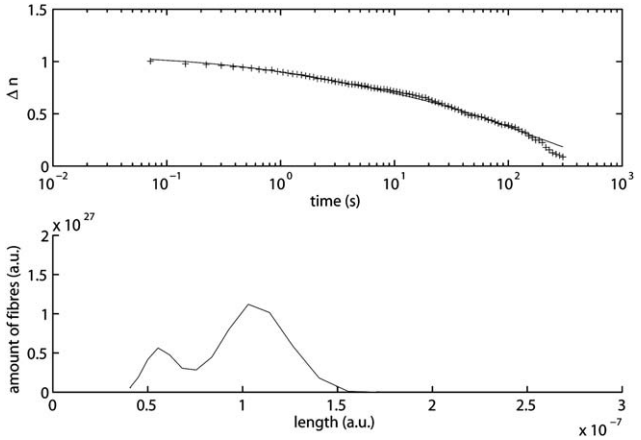

Fig. 8 A decay curve (upper graph) in which the data points are shown with plus, fitted (black line) to yield a length distribution (lower graph).

fluorescence intensity was large, but gradual. The gradual change indicates a gradual increase in the presence of DPH in hydrophobic environment, which may be caused by the larger freedom of the amphiphiles in fibres at higher temperatures. The difference in fluorescence intensity before and after heating indicated the more effective incorporation of DPH after the heating cycle.

In summary, it was found that the fibres formed from PA **1** in water are stable up to 70 °C, the temperature at which disassembly of the fibres takes place. The reassembly temperature (upon cooling) was found to be about 50 °C. The large hysteresis between disassembly (heating) and reassembly (cooling) indicates undercooling before assembly takes place and supports a nucleation-induced assembly process as is also suggested by the flow-induced birefringence measurements (*vide infra*). A second, lower, transition temperature was observed in CD and fluorescence spectroscopy. We assume a conformational change of the amphiphiles within the fibres to be the cause of this transition. Such change in either peptide packing or mobility of the alkyl tails can effectuate an increased incorporation of DPH in the hydrophobic shell of the fibre and led to an increased ellipticity signal in CD.

Dynamics of disassembly

We tried to determine the length distribution of the fibres as a function of the concentration of the PA's. If the fibrils are in dynamic equilibrium with their building blocks their length distribution can be predicted, using a general thermodynamic treatment of self-assembled structures.[44] Assuming a one-dimensional assembly, this treatment predicts that the position of peak of the length distribution should scale as $\sqrt{c}$ (where c is the concentration of the PA's). The length distribution of the fibres was measured using flow-induced birefringence, where the length distribution was derived from the decay of the birefringence signal after the cessation of the shear flow (the decay curve, D and E in Fig. 3). Unfortunately, the predicted scaling was not found. When the decay curves were fitted in order to determine the length distributions, for all samples a bimodal distribution was found (Fig. 8), independent of concentration. This also occurred when the samples were cooled slowly and left to stand for several days. This suggests that the fibres are not in thermodynamic equilibrium but in a kinetically trapped state *i.e.* although cooling was slow it was still too fast to allow the system to reach the thermodynamic lowest state. This implies the presence of an energy barrier for rearrangement of the amphiphiles within the fibres, an observation that is supported by the slow rate of disassembly (see below).

Using flow-induced birefringence also the kinetics of the disassembly of the fibres was studied. Dilution below the CAC eventually results in disassembly of fibres, although this can be a slow process. The CAC of PA **1** at room temperature is about 50 μg mL^{-1}, however, upon dilution from 100 to 25 μg mL^{-1} the flow-induced birefringence did not disappear immediately, showing that the disassembly of the fibres does not take place instantaneously. Only after 4 to 7 days (at room temperature), no birefringence signal was left. During that period, the flow-induced birefringence decreased, as was to be expected if fewer or smaller fibres were present. Directly after diluting the sample, the decay curve was measured which reflects the relaxation of the fibres from an aligned to a random orientation. Upon aging of the sample, however, the decay curve started to oscillate, suggesting the sample developed some elastic properties over time. This observation could be caused by a wide length distribution. Smaller fibres relax to random orientation and in the process 'push' larger fibres, causing a decrease in alignment (and thus in birefringence). However, larger fibres may reorient, increasing the birefringence again. Such a wide length distribution may be caused by a faster disassembly rate for smaller fibres yielding a bimodal length distribution. Unfortunately, due to these oscillations the length distribution of the fibres as a function of time could not be determined.

Thermodynamic parameters of the assembly process

In order to determine the underlying thermodynamics of the aggregation process, *i.e.* the change in Gibbs free energy ΔG, enthalpy ΔH and entropy ΔS have to be determined. Kroes-Nijboer *et al.*[45] have shown that the thermodynamic parameters of the self-assembly of β-lactoglobulin fibrils can be obtained by measuring the critical aggregation concentration as a function of temperature. Similarly, in this study we determine the thermodynamic parameters by measuring the concentration dependent disassembly temperature. The fibres were assumed to form, in essence, one-dimensional aggregates and therefore the thermodynamic theory of one-dimensional self-assembly was

applied. According to this theory, the molar fraction of fibrillar aggregates x_N consisting of N building blocks can be expressed in terms of ΔG as[44,45]

$$x_N = N(x_1 \exp(-\Delta G/RT))^N$$

where x_1 is the molar fraction of the (monomeric) building blocks, which are in our case, the individual peptide amphiphiles. Since x_N cannot exceed 1, this implies that x_1 cannot exceed exp $(-\Delta G/RT)$. This leads to the definition of the critical aggregation concentration (CAC) as $x_{1,\mathrm{CAC}} = \exp(\Delta G/RT)$. Once the concentration of the building blocks exceeds the critical aggregation concentration, all additional building blocks added will be incorporated into the fibres. The energy changes associated with the aggregation process may be derived from the temperature dependence of the CAC using the following van't Hoff equations:[45,46]

$$\Delta G = RT \ln x_{1,\mathrm{CAC}}$$

$$\Delta H = -RT^2 \left[\frac{\partial \ln x_{1,\mathrm{CAC}}}{\partial T}\right]$$

The entropy change ΔS was obtained from ΔG and ΔH using:

$$\Delta G = \Delta H - T\Delta S$$

In order to determine the thermodynamic parameters DLS was used in this study, because it allowed us to perform measurements over a large concentration range. Even though in gelled samples the signal cannot be used to determine particle size, a large change in scattering is observed when the sample disassembles. The transition temperature was taken as the inflection point of a sigmoidal curve that was fitted to the data points (see Fig. 6). At higher concentrations (2 and 5 mg mL^{-1}), the fits were poor, probably because the transition temperature was at the edge of the measured temperature range. The resulting concentration dependent disassembly temperatures are shown in Fig. 9a and the thermodynamic parameters calculated from these data in Fig. 9b–d.

The solid lines are obtained by applying the above thermodynamic theory of one-dimensional self-assembly. The change in the free Gibbs energy ΔG was found to increase at increasing temperature in line with a lower stability of the fibers at increased temperatures. Both the change in enthalpy ΔH and entropy ΔS of the assembly process were negative as well, implying that the self-assembly is an enthalpy-driven process. The value of entropy change in this process ($T\Delta S \approx -20\ RT$) indicates a significant loss in the degrees of freedom upon assembly corroborating a crystalline-like packing of the peptide amphiphiles. The value found for ΔG in this study is only slightly higher as determined for the β-lactoglobulin based fibrils ($\sim -13RT$),[45] which are considerably more resistant towards mechanical stress. It is interesting to note that although the values for ΔG are similar for both assembly processes the thermodynamics behind the self-assembly is quite different. Where the self-assembly of the peptide amphiphiles into fibres is found to be enthalpy-driven ($\Delta S < 0$, $\Delta H < 0$), the self-assembly of β-lactoglobulin into fibrils is found to be entropy-driven ($\Delta S > 0$, $\Delta H \approx 0$).

Mechanical stability

Next, we examined whether these thermally highly stable fibres were also resistant to mechanical disturbances. We studied the influence of shear flow on the fibre length distribution using flow-induced birefringence. In general, the degree of alignment and therefore the flow-induced birefringence depends on the length distribution of the fibres (the longer the fibres, the slower and the more they will be aligned in the direction of the flow) and on the shear rate (the higher the shear rate, the faster and the higher the alignment in the direction of the flow). In Fig. 10a the flow-induced birefringence during shearing (between C and D in Fig. 3) is shown for various shear rates. At the low shear rates (2 s^{-1}) the fibres did not align instantaneously. After a few minutes however, the maximum in birefringence was reached. When the shear rate was increased further to 5 s^{-1} the birefringence did not increase any further. This is in contradistinction with the fibres studied by Rogers *et al.*[42] that showed an increase in signal in a similar experiment. This difference indicates that the fibres of PA **1** were much longer than the fibres studied by

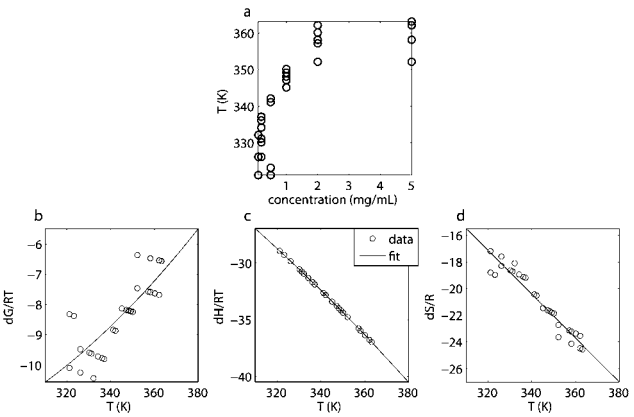

Fig. 9 Concentration dependent disassembly temperatures of PA **1** from DLS measurements and derived thermodynamic parameters. (a) Disassembly temperatures as a function of concentration. Temperature dependence of (b) free energy, (c) enthalpy and (d) entropy.

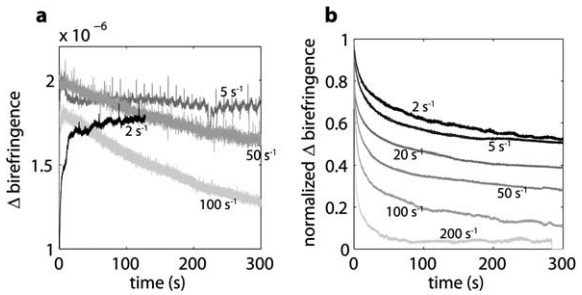

Fig. 10 Effect of shear rate. (a) Flow-birefringence decreases (for >2 s^{-1}) during prolonged shearing indicating the break-up of fibres. (b) A higher shear rate resulting in a steeper decay after the cessation of flow, indicating smaller fibres due to flow-induced break-up of fibres.

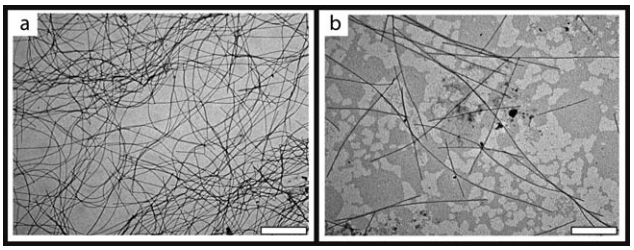

Fig. 11 TEM graphs of samples before and after applying elongational force. (a) Before treatment. (b) After treatment. The white bars represent 1 μm.

Rogers as was confirmed with TEM (see Fig. 2). On the other hand, subjecting higher shear rates (>50 s^{-1}) to the PA **1** fibres resulted in a decrease in flow-birefringence, indicating flow-induced fibre fracture as was corroborated with electron microscopy (Fig. 11). This demonstrates that these fibres have a lower tensile strength than *e.g.* fibres of β-lactoglobulin or amyloid,[26,41] that remain stable up to shear rates as high as greater than 200 s^{-1}. Damage of the fibres was corroborated by the decay curves after fast shearing (faster decay for smaller fibres, because of a faster relaxation to a random orientation—between D and E in Fig. 3). The decay curves (Fig. 10b) could be converted into fibre length distributions, which showed a shift towards smaller fibres with increasing shear rates. In order to determine absolute length scale of the fibre length distribution, the curves needed calibration, which can, in principle be achieved using TEM.[42] However, due to the high aspect ratio of the fibres of self-assembled PA **1**—they are long, but very thin—the length of the fibres could not be determined with TEM. At large magnification the fibres were detectable but stretched beyond the visible area, while at lower magnification the very thin fibres could not be resolved (Fig. 2). Therefore, in our case the flow-birefringence measurements could not be calibrated and only relative length distributions could be determined. Furthermore, fibres of PA **1** showed fast recovery—an hour after shearing decay curves overlapped with those before fast shearing (data not shown)—which hampered TEM sample preparation of the broken fibres.

Conclusions

For PA **1** the derived critical aggregation concentration was found to be about 50 μg mL^{-1} (55 μM). Above this concentration, PA **1** assembled into fibres in a kinetically trapped state. Dilution of a fibre-containing solution below the CAC did not result in instantaneous disassembly—only after a few days the amphiphiles were completely dissolved. This slow disassembly indicates a kinetically trapped architecture, induced by the presence of energy barriers. The fibres were found to fracture readily upon application of a tensile force caused by the elongational component of the applied shear flow. Contrastingly, upon heating the fibres did not disassemble until a temperature of 70 °C. Cooling down the dissolved PAs, reassembly was observed around 50 °C. This large hysteresis suggests a nucleation-induced assembly process. A second transition temperature was observed at 50 °C and 30 °C upon heating and cooling, respectively. This transition is assumed to be associated with a conformational change in the peptide and/or an increase in mobility of the alkyl tails. By measuring the critical aggregation concentration as a function of temperature the thermodynamic parameters were determined and the self-assembly process was found to be enthalpy driven.

Experimental

Fibre preparation

The amphiphiles were dispersed in Milli-Q, heated to 50 °C for 30 min, followed by 15 min sonication at that temperature. Subsequently, the samples were heated to 90 °C and allowed to cool to room temperature.

Flow-induced birefringence

The flow-induced birefringence experiments were performed on a strain-controlled ARES rheometer (Rheometrics Scientific) equipped with an optical analysis module. The system has undergone adjustments by Klein *et al.*[47] to increase the sensitivity and reduce the background signal (residual birefringence in the optical train). All measurements were performed in Couette geometry with a static inner bob diameter of 32 mm and rotating outer cup diameter of 33.8 mm. A laser beam of wavelength 670 nm passes through the gap between the cup and bob through 20 mm of sample. In this set-up, the apparatus was capable of measuring birefringence down to 10^{-8} at a sampling frequency of 24 Hz. The geometry required 12 mL of sample.

Fluorescence spectroscopy

Fluorescence measurements were performed on a Perkin Elmer LS-55 fluorescence spectrometer. The excitation wavelength was 362 nm, and the emission was recorded between 360 and 550 nm, while the maximum extinction at 429 nm was used to determine a change in fluorescence. The spectra were recorded at a speed of 300 nm min^{-1}. Both excitation and emission slit parameters were set to 2.5.

CAC measurements. 1.00 μL of a solution of DPH (1,6-diphenyl-1,3,5-hexatriene, 10 mM in THF)[43] was added to samples of PA **1** with a volume of 1.50 mL and a concentration of 1000, 500, 200, 100, 50, 20, 10, 5, 2 and 1 μg mL^{-1}. After addition of DPH, the sample containers were wrapped in aluminium foil to exclude light, and the fibres were prepared following the standard procedure.

Temperature measurement. To 1.50 mL fibre sample of 1.0 mg mL^{-1} PA **1**, prepared following the standard procedure, 1.00 μL of 10 mM DPH in THF was added. The sample was left in the dark for 1 h. The samples were heated from 20 to 90 °C for about 30 min using a water bath connected to the spectrometer and cooled in the same way.

Circular dichroism (CD) spectroscopy

The spectra were recorded on a JASCO J-810 spectropolarimeter.

CAC measurements. Samples with a concentration PA **1** of 1000, 800, 600, 400, 200, 100, 80, 60, 40, 20, 10, 8, 6, 4, 2 and 1 μg mL^{-1} were prepared following the standard procedure. The CD measurements were performed from low to high concentrations, starting with a 1 cm path length quartz cell, and switching to 1.00 mm and 0.20 mm path length quartz cells when the high tension signal was higher than 800 during the measurements. Spectra were recorded from 265 to 185 nm, using a scanning speed of 100 nm min^{-1} and a 0.5 nm data point interval.

Temperature measurements. The measurements were carried out at a concentration of 0.20 mg mL^{-1} prepared following the standard procedure using a 1.00 mm quartz cell. A heating or cooling rate of 3 °C min^{-1} was used, and the ellipticity at 196 nm was measured between 10 and 90 °C.

Transmission electron microscopy (TEM)

TEM samples were prepared by floating a carbon-coated copper grid on a peptide amphiphile solution of either 1.0 or 0.20 mg mL^{-1} for 5 min, followed by removal of residual solution by blotting with a paper filter. The samples were visualized using a JEOL 1010 transmission electron microscope set on an accelerating voltage of 60 kV.

Dynamic light scattering (DLS)

DLS measurements were performed on a Zetasizer Nano S (Malvern Instruments Ltd, England). Every 5 °C between 10 and 90 °C the sample was equilibrated for 5 min before a measurement in triplicate was performed. Every measurement consisted of 6 runs of 6 s, with a measurement position of 4.65 and a set attenuation of 7. At least two different samples at each concentration were used for these experiments.

Acknowledgements

We thank Pieter Nieuwland for the 3D-drawings.

References

1 I. W. Hamley, *Angew. Chem., Int. Ed.*, 2007, **46**, 8128–8147.
2 D. W. P. M. Löwik and J. C. M. van Hest, *Chem. Soc. Rev.*, 2004, **33**, 234–245.
3 H. G. Cui, M. J. Webber and S. I. Stupp, *Biopolymers*, 2009, **94**, 1–18.
4 E. Kokkoli, A. Mardilovich, A. Wedekind, E. L. Rexeisen, A. Garg and J. A. Craig, *Soft Matter*, 2006, **2**, 1015–1024.
5 D. W. P. M. Löwik, E. H. P. Leunissen, M. van den Heuvel, M. B. Hansen and J. C. M. van Hest, *Chem. Soc. Rev.*, 2010, **239**, 3394–3412.
6 A. Aggeli, I. A. Nyrkova, M. Bell, R. Harding, L. Carrick, T. C. B. McLeish, A. N. Semenov and N. Boden, *Proc. Natl. Acad. Sci. U. S. A.*, 2001, **98**, 11857–11862.
7 S. Cavalli and A. Kros, *Adv. Mater.*, 2008, **20**, 627–631.
8 S. Cavalli, F. Albericio and A. Kros, *Chem. Soc. Rev.*, 2010, **39**, 241–263.
9 S. Cavalli, J. W. Handgraaf, E. E. Tellers, D. C. Popescu, M. Overhand, K. Kjaer, V. Vaiser, N. Sommerdijk, H. Rapaport and A. Kros, *J. Am. Chem. Soc.*, 2006, **128**, 13959–13966.
10 N. Nakashima, S. Asakuma and T. Kunitake, *J. Am. Chem. Soc.*, 1985, **107**, 509–510.
11 N. Yamada, K. Ariga, M. Naito, K. Matsubara and E. Koyama, *J. Am. Chem. Soc.*, 1998, **120**, 12192–12199.
12 E. Jahnke, I. Lieberwirth, N. Severin, J. P. Rabe and H. Frauenrath, *Angew. Chem., Int. Ed.*, 2006, **45**, 5383–5386.
13 J. D. Hartgerink, E. Beniash and S. I. Stupp, *Science*, 2001, **294**, 1684–1688.
14 J. D. Hartgerink, E. Beniash and S. I. Stupp, *Proc. Natl. Acad. Sci. U. S. A.*, 2002, **99**, 5133–5138.
15 S. E. Paramonov, H. W. Jun and J. D. Hartgerink, *J. Am. Chem. Soc.*, 2006, **128**, 7291–7298.
16 J. T. Meijer, M. Roeters, V. Viola, D. W. P. M. Lowik, G. Vriend and J. C. M. van Hest, *Langmuir*, 2007, **23**, 2058–2063.
17 D. W. P. M. Löwik, J. Garcia-Hartjes, J. T. Meijer and J. C. M. van Hest, *Langmuir*, 2005, **21**, 524–526.
18 Y. C. Yu, M. Tirrell and G. B. Fields, *J. Am. Chem. Soc.*, 1998, **120**, 9979–9987.
19 Y. C. Yu, P. Berndt, M. Tirrell and G. B. Fields, *J. Am. Chem. Soc.*, 1996, **118**, 12515–12520.
20 S. R. Bull, M. O. Guler, R. E. Bras, P. N. Venkatasubramanian, S. I. Stupp and T. J. Meade, *Bioconjugate Chem.*, 2005, **16**, 1343–1348.
21 S. R. Bull, M. O. Guler, R. E. Bras, T. J. Meade and S. I. Stupp, *Nano Lett.*, 2005, **5**, 1–4.
22 G. A. Silva, C. Czeisler, K. L. Niece, E. Beniash, D. A. Harrington, J. A. Kessler and S. I. Stupp, *Science*, 2004, **303**, 1352–1355.
23 E. F. Banwell, E. S. Abelardo, D. J. Adams, M. A. Birchall, A. Corrigan, A. M. Donald, M. Kirkland, L. C. Serpell, M. F. Butler and D. N. Woolfson, *Nat. Mater.*, 2009, **8**, 596–600.
24 J. M. Anderson, M. Kushwaha, A. Tambralli, S. L. Bellis, R. P. Camata and H. W. Jun, *Biomacromolecules*, 2009, **10**, 2935–2944.
25 M. Zhou, A. M. Smith, A. K. Das, N. W. Hodson, R. F. Collins, R. V. Ulijn and J. E. Gough, *Biomaterials*, 2009, **30**, 2523–2530.
26 V. Castelletto, I. W. Hamley, J. Perez, L. Abezgauz and D. Danino, *Chem. Commun.*, 2010, **46**, 9185–9187.
27 E. K. Hill, B. Krebs, D. G. Goodall, G. J. Howlett and D. E. Dunstan, *Biomacromolecules*, 2006, **7**, 10–13.
28 H. J. Schnittler, S. W. Schneider, H. Raifer, F. Luo, P. Dieterich, I. Just and K. Aktories, *Pfluegers Arch.*, 2001, **442**, 675–687.
29 J. F. Smith, T. P. J. Knowles, C. M. Dobson, C. E. MacPhee and M. E. Welland, *Proc. Natl. Acad. Sci. U. S. A.*, 2006, **103**, 15806–15811.
30 J. D. Clay and K. W. Koelling, *Polym. Eng. Sci.*, 1997, **37**, 789–800.
31 J. A. Odell and A. Keller, *J. Polym. Sci., Part B: Polym. Phys.*, 1986, **24**, 1889–1916.
32 A. Kroes-Nijboer, P. Venema, H. Baptist and E. van der Linden, *Langmuir*, 2010, **26**, 13097–13101.
33 C. Akkermans, P. Venema, S. S. Rogers, A. J. van der Goot, R. M. Boom and E. van der Linden, *Food Biophys.*, 2006, **1**, 144–150.
34 C. Cerami, U. Frevert, P. Sinnis, B. Takacs, P. Clavijo, M. J. Santos and V. Nussenzweig, *Cell*, 1992, **70**, 1021–1033.
35 D. C. Duncan and D. G. Whitten, *Langmuir*, 2000, **16**, 6445–6452.
36 D. W. P. M. Löwik, I. O. Shklyarevskiy, L. Ruizendaal, P. C. M. Christianen, J. C. Maan and J. C. M. van Hest, *Adv. Mater.*, 2007, **19**, 1191–1195.
37 M. van den Heuvel, D. W. P. M. Löwik and J. C. M. van Hest, *Biomacromolecules*, 2008, **9**, 2727–2734.
38 M. van den Heuvel, D. W. P. M. Löwik and J. C. M. van Hest, *Biomacromolecules*, 2010, **11**, 1676–1683.
39 M. van den Heuvel, A. M. Prenen, J. C. Gielen, P. C. M. Christianen, D. J. Broer, D. W. P. M. Löwik and J. C. M. van Hest, *J. Am. Chem. Soc.*, 2009, **131**, 15014–15017.
40 C. Akkermans, A. J. Van Der Goot, P. Venema, H. Gruppen, J. M. Vereijken, E. Van Der Linden and R. M. Boom, *J. Agric. Food Chem.*, 2007, **55**, 9877–9882.
41 A. W. Chow and G. G. Fuller, *Macromolecules*, 1985, **18**, 786–793.
42 S. S. Rogers, P. Venema, L. M. C. Sagis, E. van der Linden and A. M. Donald, *Macromolecules*, 2005, **38**, 2948–2958.
43 A. Riepe, H. Beier and H. J. Gross, *FEBS Lett.*, 1999, **457**, 193–199.
44 J. Israelachvili, *Intermolecular and Surface Forces*, Academic Press, 2nd edn, 1992.
45 A. Kroes-Nijboer, P. Venema, J. Bouman and E. van der Linden, *Food Biophys.*, 2009, **4**, 59–63.
46 J.-A. Yu, S.-H. Oh, Y.-R. Park and J.-S. Kim, *Macromol. Symp.*, 2007, **249–250**, 445–449.
47 C. Klein, P. Venema, L. Sagis, D. van Dusschoten, M. Wilhelm, H. W. Spiess, E. van der Linden, S. S. Rogers and A. M. Donald, *Appl. Rheol.*, 2007, 17.